

A New Perspective and Explanation for the Formation of Plasmaspheric Shoulder Structures

Hua Zhang¹ Guangshai Peng¹ Chao Shen² Wu Yewen¹

¹Institute of Space Weather, Nanjing University of Information Science & Technology, Nanjing, China.

²Harbin Institute of Technology, Shen Zhen, China.

Correspondence to: Hua Zhang (289534957@qq.com)

Abstract

Over the hours of 5-9 UT on 8 June 2001, the extreme ultraviolet (EUV) instrument onboard IMAGE satellite observed a shoulder-like formation in the morning sector and a post-noon plume-like structure. The plasmopause formation is simulated using the Test Particle Model (TPM), based on a drift motion theory, which reproduces various plasmopause structures and evolution of the shoulder feature. The analysis indicates that the Shoulder is created by sharp reduction and spatial non-uniform in the dawn-dusk convection electric field intensity. The TPM modeled event is found to develop an initial pre-dawn asymmetric bulge that becomes a shoulder as a result of increased “co-rotation” rate with increasing L-shell that is preceded by localized outward convection. The shoulder structure rotates sunward and develops into a single or double plume structure during an active time period in simulation.

Keywords: plasmopause; shoulder-like; plume-like; IMAGE/EUV

1. Introduction

The plasmasphere is an important region in the inner magnetosphere, surrounding the Earth and extending to 5 Earth radii(R_E), which contains dense(10 - 10000 cm^{-3}) and cold plasma (below 1eV). The plasmopause is formed by a superposition of corotation and convection electric field in the inner magnetosphere (Nishida, 1966; Chen and Wolf, 1972). The formation and size of plasmopause vary with a geomagnetic activity level. Generally, as the disturbance level increases, the plasmopause position moves closer to the Earth and of shape deviates from circle in

29 the equatorial plane (Grebowsky, 1970). Atypical plasmopause structures, such as
30 ‘bulge’ and plume, occur often in both whistler and in-situ data (Carpenter and
31 Anderson, 1992). There are many theoretical research **studies** to explain the formation
32 of plume (Grebowsky, 1970; Pierrard and Lemaire, 2004; Zhang et al., 2013), and
33 Pierrard and Cabrera (2006) firstly simulated a double-plume , but **did not explain** the
34 origin of second-plume.

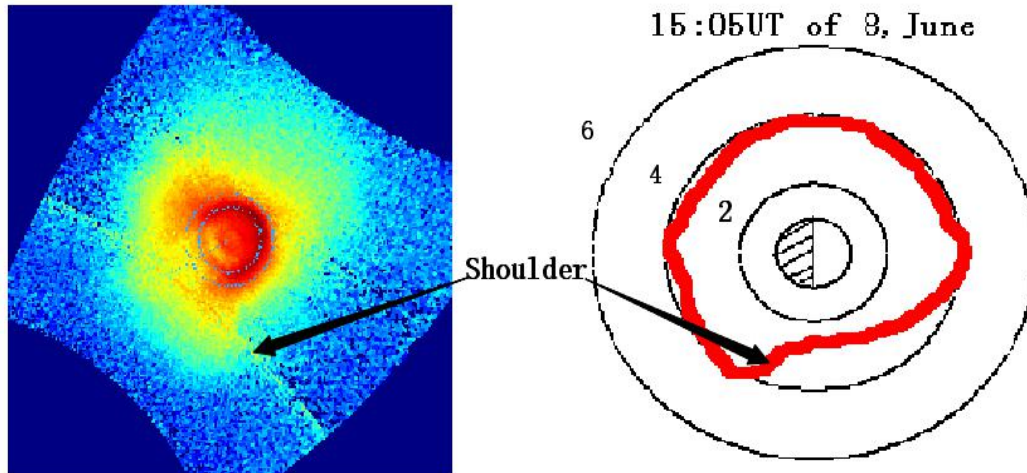
35 The EUV instrument onboard IMAGE satellite was launched in March 2000, **that**
36 provided a global perspective **of** the plasmasphere. **Such** as plume, finger, notch and
37 shoulder, and so on, **were** observed by EUV (Sandel et al., 2001). One of
38 plasmaspheric structures, shoulder, **has been less studied** in the previous papers than
39 plume. **However**, the shoulder may play an important role in a loss mechanism for
40 ring current (Burch et al., 2001). So, it is important to study the formation
41 mechanism of the shoulder.

42 At present, there are no convincing explanations for the dynamic formation of
43 shoulder. Goldstein et al.(2002) firstly proposed an explanation, based on the
44 Magnetospheric Specification Model(MCM) simulation output, for the formation of
45 shoulder. They proposed that the shoulder is created by **a** sudden decrease of
46 dusk-dawn electric field. As the interplanetary magnetic field (IMF) turns northward
47 from southward, **it triggers** anti-sunward flow of plasma in the predawn sector, to
48 produce an asymmetric bulge called shoulder. Later, based on physical mechanism of
49 interchange instability and a Kp-dependent E5D electric field model, Pierrard and
50 Lemaire (2004) suggested that the shoulder is not the result of radial outflow of
51 plasma, same as the presentation of Goldstein et al. (2002), but is inward plasma
52 drift in post-midnight sector.

53 Then, scarce papers about dynamical formation of the shoulder are delivered than
54 of the plume. In this paper, we used TPM to simulate dynamical formation of the
55 shoulder, using Weimer’s statistical E-field (Weimer, 2001; Zhang et al., 2012),
56 which is both spatially nonuniform and dynamically responsive to change
57 geomagnetic and solar wind conditions. To drive the TPM model, several inputs are
58 used: Dst, solar wind (SW) and interplanetary magnetic field (IMF) data sets. The

59 authors make an attempt to propose a new convincing explanation for the formation
60 of the shoulder-like structure, different from the previous explanations.

61 2. Shoulder Observation



62
63 **Figure1. Snapshot of plasmasphere (left panel) by EUV instrument, at 15:05 UT of 8 June 2001,**
64 **Sunlight is an incident from the upper right. Earth is in the center of panels and shoulder is**
65 **observed and labeled in the snapshot. The right panel is plasmopause that is extracted from the**
66 **left plasmapheric image.**

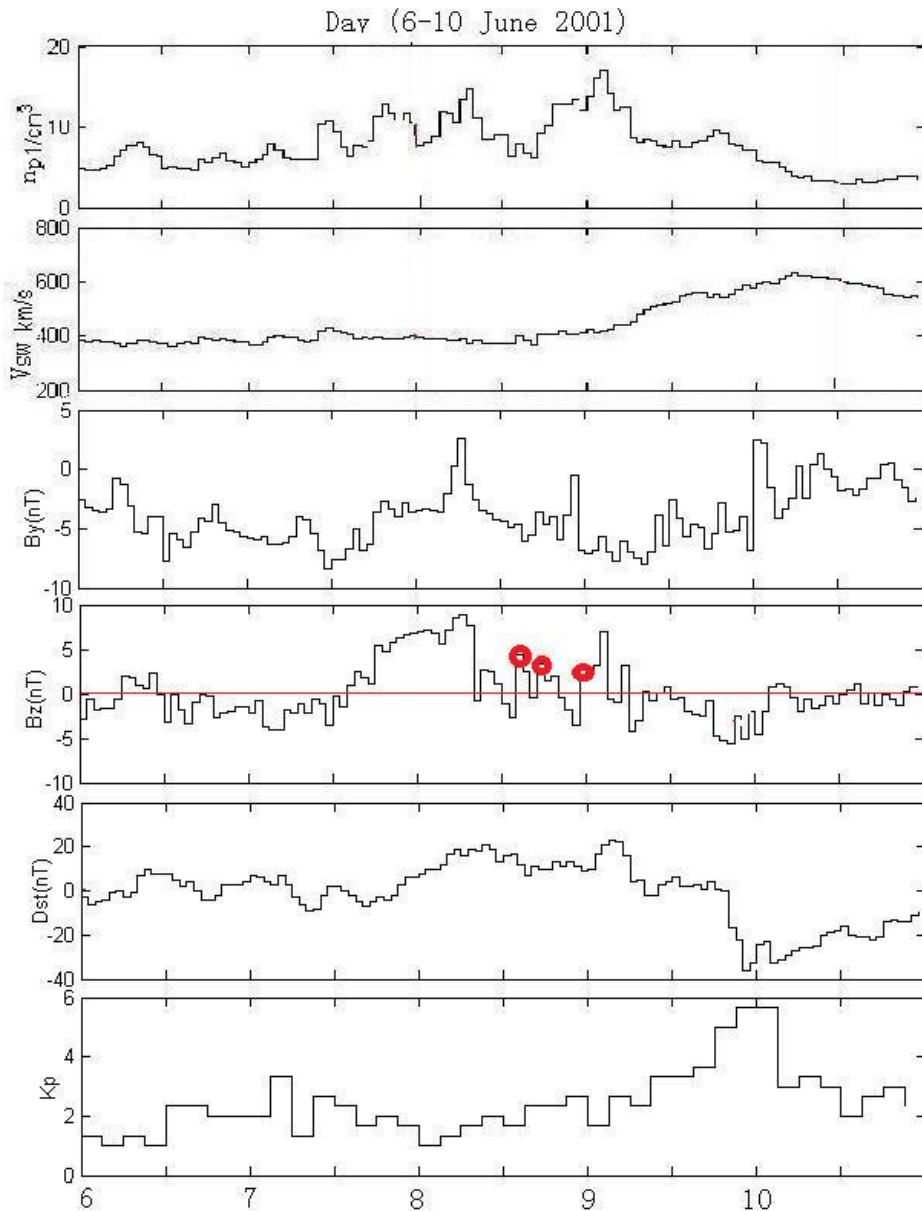
67 Figure 1 illustrates the shoulder-like structure, a sharp radial plasmaspheric
68 structure about 1 RE radial extension, in the post-midnight sector, which was viewed
69 by EUV imager onboard IMAGE satellite at 15:05 UT of 8 June 2001. The right panel
70 illustrates the plasmopause extracted from the left panel in Figure 1. The outer
71 boundary of plasmasphere is assumed to be 40% of maximum brightness of 30.4nm
72 He⁺ emission, where the intensity is the logarithm of the luminosity (Pierrard and
73 Cabrera, 2006). Then, the shoulder-like is labeled and marked by arrows in the plot.
74 Comparison of sequential observations with the simulation pictures, show that the
75 shoulder structure corotating with the main plasmaspheric body can be seen in Figure
76 3, and is discussed in the next section. That means the outer edge of the shoulder
77 corotates faster than the inner edge in development phase (Goldstein et al., 2002).
78 Then, the shoulder moves eastward to the afternoon sector and evolves into the
79 plume-like structure. Over the next hours, the outer body of plume flows sunward
80 from noon sector, and results in the plume thinning out and disappearing (can see the

81 simulation of Figure 3). In the next section, we take the case of 8 June 2001
82 observation as an example, to discuss the simulation of the Shoulder and the plume
83 evolution based on the TPM method.

84 **3. Simulation**

85 In the region of plasmasphere occupied, charged particles are cold plasma (e.g.
86 energy of particles is $< 1\text{eV}$). So, we can assume that plasma elements have only $\mathbf{E} \times$
87 \mathbf{B}/B^2 drift motions (Li and Xu, 2005; Lejosne and Mozer, 2016). Here, the electric
88 field intensity of E-model is superposition of convection and corotation electric field.
89 The electric field plays a key role in plasma drift motion and the formation of
90 plasmasphere (Pierrard et al., 2008). In the present paper, the Weimer's electric field
91 (Weimer, 2001) is mapped into the magnetosphere along magnetic lines to model the
92 magnetospheric convection electric field (Zhang et al., 2012), and T96 magnetic field
93 to model the background magnetic field.

94 In the simulation, the calculation **region** is radial range of 2-7 R_E and azimuthal
95 span $0-359^\circ$. Dispersion by iso-spacing grids that correspond to the radial and
96 azimuthal steps are equal to $0.1R_E$ and 1° respectively, in the magnetic equatorial
97 plane. Ten particles are placed into each grid, so particle density is proportional to L^{-1}
98 which is not consistent with the actual density in a saturation state (close to true
99 density presumably is proportional to L^{-4}), but is adequate to study the evolution of
100 plasmaspheric morphology using a skeleton map of particles during a substorm period.
101 The TMP runs 3 days under the low activity condition to obtain the boundary
102 conditions for the simulation.



103

104 **Figure 2. Input parameters of the TPM model, the variation of the By and Bz component of the**

105 **IMF, the Dst index and Kp index, on 6 -10 June 2001, is a typical substorm case.**

106 The paper presents the case of 8-9 June 2001, to study the evolution of the

107 shoulder and propose a hypothetical explanation produced by TPM simulation.

108 During the geomagnetic substorm, all the TPM inputs are available. IMF and

109 Solar Wind data are available in ACE satellite data center, and Dst index can be

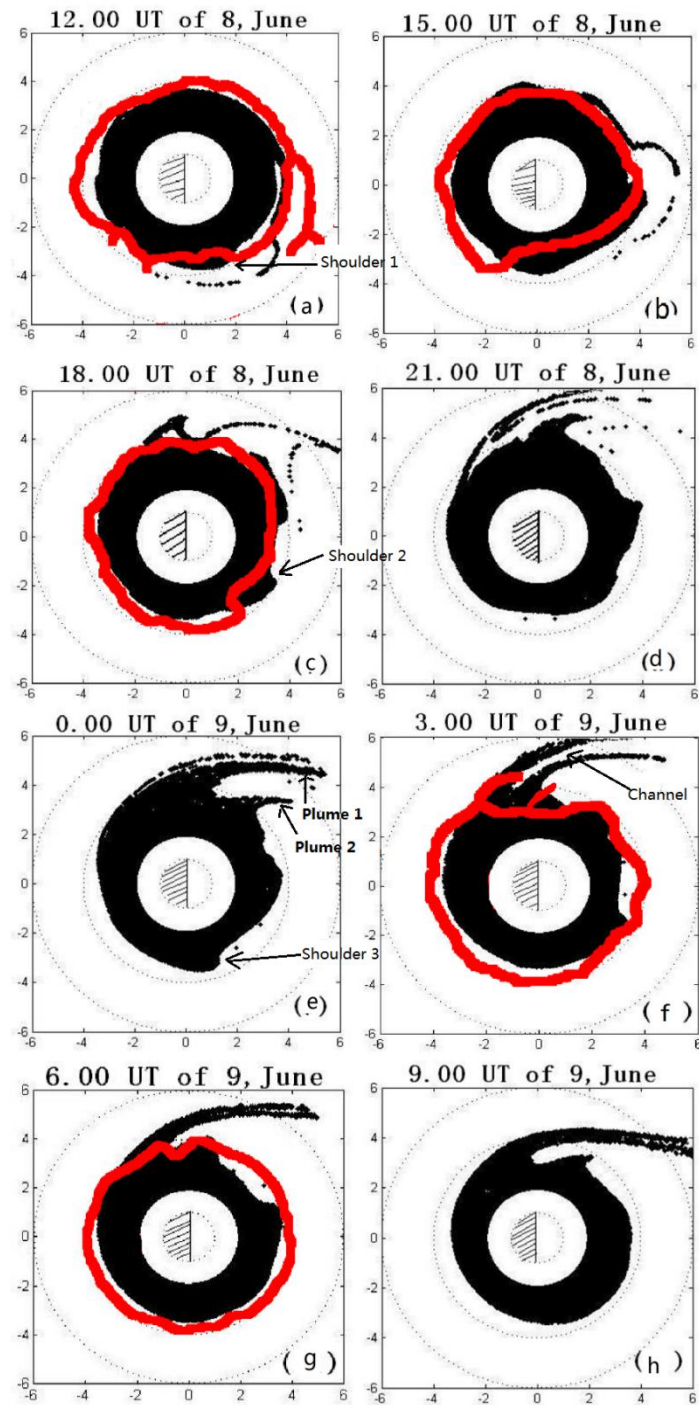
110 seen in World Data center for Geomagnetism, Kyoto. Fig.2 shows the By, Bz

111 components of the IMF, the Dst index and the geomagnetic activity index Kp,

112 observed from 6 to 10 June 2001. This is a typical substorm case where the Kp

113 index gradually increases up to 5+ and then decreases. The TPM runs with

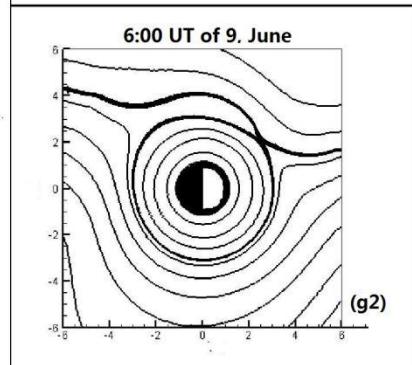
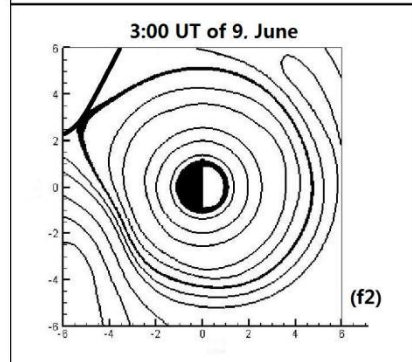
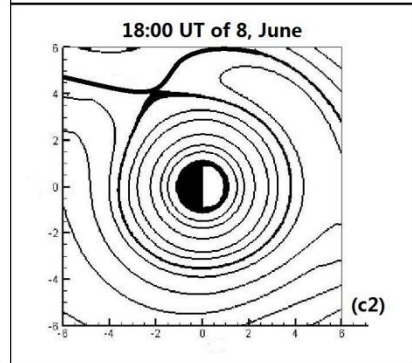
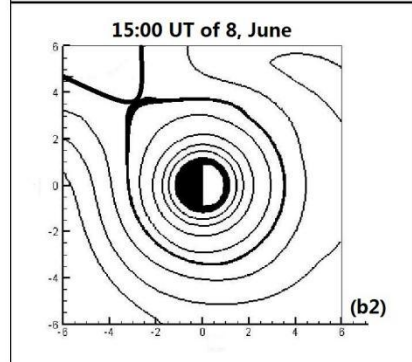
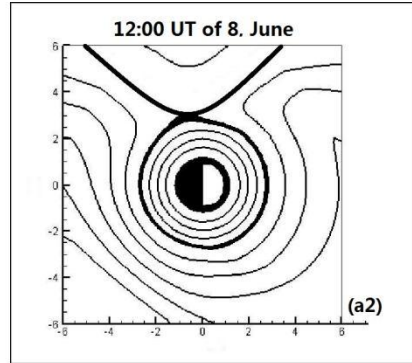
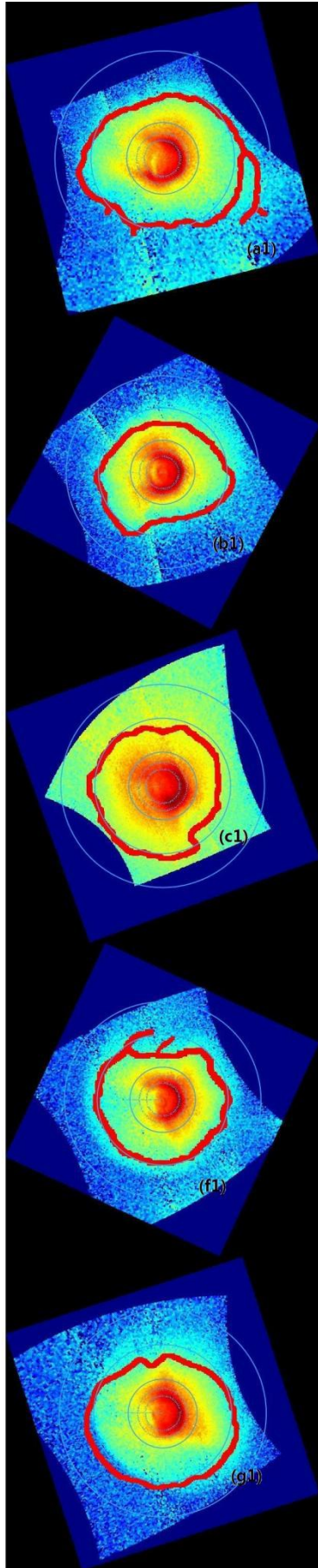
114 3-minute time resolution from 6 June at 00:00 UT to 10 June at 12:00 UT. The
115 results of simulation are shown in Fig.3, whose corresponding times are labeled
116 on the title of each panel. The **simulated plasmopause** is a skeleton which consists
117 of continuous **particle** distribution. Comparison of TPM simulation (black body)
118 and EUV observation (red line) in Fig.3 **indicates that** the simulated plasmopause
119 positions correspond generally rather favorable with the EUV observations. The
120 results of EUV observation show that the plasmopause is seldom smooth or
121 irregular, due to the fluctuations in plasmopause region caused by successive
122 particles injection during a disturbance period (Goldstein et al., 2002; Gallagher et
123 al., 2005), in agreement with previous whistler observations (Carpenter and
124 Anderson, 1992). **In contrast**, the simulation of plasmapauses by TPM is **more**
125 smooth. So, observations and simulations are not identical, due to deviation in the
126 extraction of the boundary from EUV image and optical contamination of the
127 image (Sandel et al., 2001; Zhang et al., 2013) and the limitation in the TPM
128 model and the unrealistic Weimer electric field model. .



129

130 **Figure 3.** The simulation of plasmaspheric morphology compared with EUV/IMAGE observation in the
 131 geomagnetic equatorial plane on 8 - 9 June 2001. The red irregular curves indicate plasmopause
 132 observation by EUV/IMAGE. Black contours are the plasmasphere simulated by the TPM model. White
 133 contours are the main plasmasphere (located at 1-2 Re region). The dotted circles on the panels
 134 correspond to L=1, 2, 4 and 6.

135



137 Figure 4. The subscript of panels correspond to Figure 3. The left column of panels show **original**
138 observation results by EUV/IMAGE, the blue circles on the panels correspond to L=1, 2, 4 and 6. The right
139 column of panels show equipotential lines in the equatorial plane, the last closed equipotential (LCE) is
140 the bold black curve.

141 Panels of Fig.3(a) - (h) illustrate the plasmasphere obtained on the interval of from
142 **at 12:00 UT on 8 June to at 09:00 UT on 9 June in 2001 with snapshots every three**
143 **hours**. Figure4 illustrates **original** observations by EUV/IMAGE and equipotential
144 lines in the equatorial plane. When the Kp index increased, the last closed
145 equipotential shifts closer to the Earth. The results of the simulation show the
146 evolution and development of the features of the plasmopause, like shoulders and
147 plumes. One can see that the plasmopause is closer to the Earth in the predawn sector.
148 The reason is the increase of rotation velocity resulting in plasmopause of inward flow
149 in the predawn sector (Pierrard and Cabrera, 2006; Verbanac et al., 2018). At 15:05
150 UT of 8 June, the TPM simulation captures an infant shoulder-like structure in panel
151 Fig.3 (b), and then corotates with the plasmasphere body moved eastward and further
152 reproduces a mature shoulder formation in Fig.3(c). The overall agreement between
153 TPM simulation and EUV observed is quite well, but the TPM shoulder is located
154 ~1.5 hours earlier in magnetic local time (MLT) that probably originated from the
155 convection electric field model (Goldstein et al., 2002; Pierrard and Cabrera, 2005;
156 Zhang et al., 2013).

157 The EUV observation illustrated in Fig.3 (f) shows that a plume is indeed observed
158 in the afternoon or dusk sector. The results of the simulation also reproduce the
159 formation and the evolution of the plumes, which derives from the shoulder structure
160 in this case, illustrated in panels of Fig.3 (d)-(f). The simulation shows that the
161 shoulders generate in the post-midnight sector (Verbanac et al., 2018), and then
162 rotates eastward around the Earth to the afternoon sector (Goldstein et al., 2002).
163 When the level of geomagnetic activity increases, the plasma element in the shoulder
164 around the outer plasmasphere would **convect** outward and then into the dayside
165 magnetopause (Li and Xu, 2005; Pierrard et al., 2008), and produce the plasmaspheric
166 plume structure. The shoulder1 firstly arises on Fig.3(a) in the morning sector (at 12

167 UT, 8 June 2001), and then corotates with the main body of the plasmasphere to the
168 afternoon sector on Fig.3(c) (at 18 UT, 8 June 2001). During this period, the Kp index
169 increases to 3+ from 1 (see in Fig.2), and magnetosphere convection is slightly
170 enhanced that triggers plasma elements in the shoulder1 doing sunward convection,
171 then produces the plume1 at 21 UT on 8 June 2001 (see in Fig.3(d)). The mature
172 shoulder2, illustrated in Fig.3(b), corotates eastward with the Earth to the
173 afternoon-dusk sector. During the period of 0-3 UT on June 9, the Kp index gradually
174 increases up to 5+, indicating that magnetospheric convection is enhanced and the
175 convective electric field increases. The infantile plume2, illustrated in the panel of
176 Fig.3(e), derives from outflow of plasma elements in the shoulder2, and evolves into
177 the mature plume2 in Fig.3(f). Later, the double-plumes formation that is extended
178 from the plasmopause to the magnetosphere, is presented in the simulation results in
179 panels of Figs.3 (e)-(f).

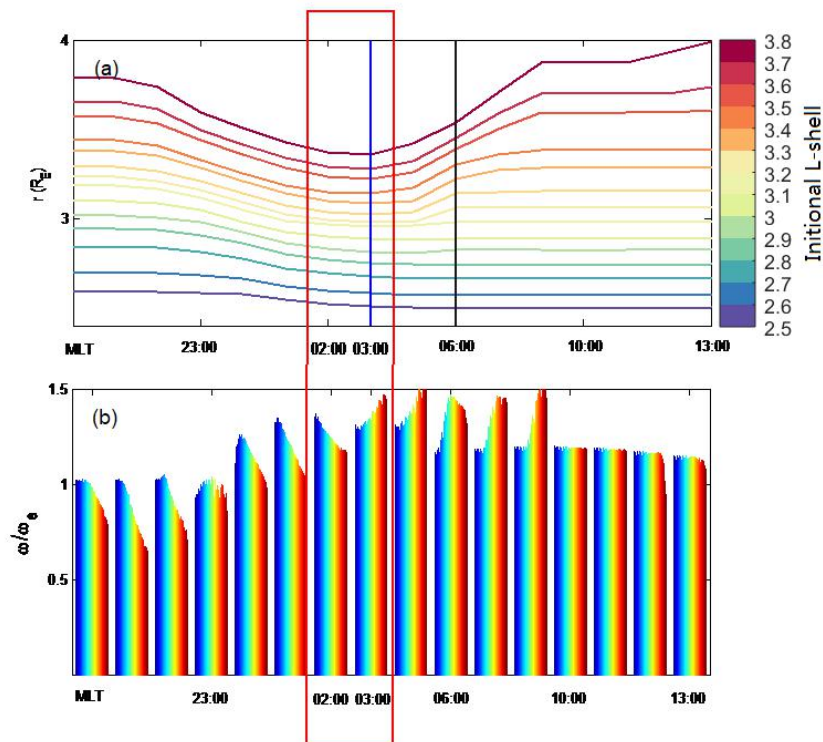
180 The cavity in between the double plumes, or between plumes and the main body
181 of plasmasphere, may be responsible for the formation of channel and notch structures
182 (Gallagher et al., 2005). The base and the westward edge of the plume are connected
183 with the main body of plasmasphere. Moreover, there is a cavity topology, a
184 low-density region, between the tail structure of the plasmasphere and the main body
185 of plasmasphere. That is the channel structure of the plasmasphere. The plume
186 corotates with the Earth, becomes thinner, and finally disappeared (Li and Xu, 2005).
187 The results of simulation reproduce the channel structure in Fig.3(f). Gallagher et al.
188 (2005) proposes that notches and channels share the same origin, which derive from a
189 low-density cavity in the dusk region during recovery at the base of the plasmaspheric
190 plume. The absence of notch structure in this simulation event is due to the fact that
191 the potential structure does not cause the inward flow of plasma in the afternoon
192 sector, and the low disturbance time is maintaining for not long enough.

193 By contrastive analysis on between Fig.2 and Fig.3, the formation of the
194 shoulder is produced during the intensity of the convection electric field suddenly
195 decrease (Goldstein et al., 2002; Pierrard and Lemaire, 2004), when IMF sudden turns
196 northward from southward. There are three shoulders reproduced during this substorm

197 period, depicted in panels of Fig.3 (b)-(g). The time of the shoulder appearance is
198 labeled by three red circles in Fig.2, at 14:00 UT, 17:00 UT, 23:00 UT on 8 June
199 respectively. At that moment, the Bz component of the IMF turns northward. But not
200 all of the times, the Bz component of the IMF **that** turns northward could produce the
201 shoulder structure. One can see that no shoulders were reproduced in the results of the
202 simulation, at 02:00 UT, 05:00 UT, and 08:00 UT on 9 June 2001 respectively. The
203 Bz value of southward component must be less than the previous 24-hours mean
204 value. The intensity of the convection electric field is greater than the previous
205 24-hours level. So the last closed equipotential line (LCE) would be closer to the
206 Earth and result in plasmopause of inward flow in the predawn sector (Zhang et al.,
207 2013).

208 **4. Discussion**

209 The physical explanation of shoulder formation is not yet understood. In the present
210 section, we use the case of Figure 1 as an example to investigate the physical
211 mechanism of shoulder formation based on the TPM model. Fourteen test particles
212 are placed in the range of $2.5 \leq L \leq 3.8$, initial position located at 12:00 MLT, space step
213 takes $0.1R_E$, and then trace these particles' motion. **Outputs are the trajectory (see in**
214 **Fig.5(a)) and the rotation rate (see in Fig.5(b)) of these test particles corresponding to**
215 **given magnetic local time illustrated in the bottom of Fig.5.**



216

217 **Figure 5. The trajectory (upper plot) and the rotation rate (bottom plot) of 14 test particles**
 218 **corresponding to MLT (location-dependent) during a substorm. The legend indicates fourteen test**
 219 **particles of various initial L-shell. The day is 8 June 2001.**

220 The top panel shows that the outer part of plasmasphere ($L > 3.3$ Re) drifts inward
 221 **before 02 MLT**, and moves outward (could reach up to 3.9 Re position) in the
 222 predawn sector (after 03:00 MLT sector) (Verbanac et al., 2018). The radial motion of
 223 inner plasmasphere ($L < 3.3$) is negligible. **The shoulder is forming across 03-06 MLT**
 224 **region** (between blue vertical line and black vertical line in Figure 5(a)). The
 225 outermost particle moves outward 0.7 Re, and the fourth particle moves outward 0.45
 226 Re, from 03:00 MLT to 08:00 MLT. So, the shoulder has a sharp eastern edge about
 227 0.2Re~0.3Re in radial extension and across a narrow 3-5 hours MLT region.
 228 Goldstein et al.(2002) proposed the shoulder formation by an outward radial motion
 229 of plasma in a narrow range and in the morning sector. **The simulation of this paper**
 230 **verifies the conclusions of Goldstein (2002) and Verbanac (2018).**

231 The lower panel shows the corotational angular velocity of test particles in the
 232 range of $2.5 < L < 4.0$. The simulation results suggest that plasma element in

233 plasmasphere region rotation speed varies significantly with radial distance (Galvan,
234 2010). The inner part of plasmasphere rotates faster than its outer part before 02:00
235 MLT sector, vice versa in a range of in the 03:00-08:00 MLT sector [Lejosne and
236 Mozer, 2016]. The previous researchers analyzed the EUV observation and proposed
237 the shoulder structure has MLT sharpening in the angular direction. It indicates that
238 the outer edge of the shoulder rotates faster than the inner edge, resulting in
239 steepening of the MLT-profile of the shoulder (Goldstein et al., 2002). The lower
240 panel shows, with the increase of L, the rotation rate of the plasmasphere tends to
241 slightly decrease on the dusk side and obviously increase on the dawn side.

242 Fig. 5 indicates, in the region of 21:00 - 23:00:00 MLT, that the rotation rate is
243 about corotation in the inner plasmasphere ($L < 3$), but is the interval of 70% - 90% of
244 corotation in the outer plasmasphere ($L > 3$). The rotational value decreases with the
245 increase of L [Galvan et al., 2010]. Gallagher et al. (2005) investigates the drift rate of
246 notches in the geomagnetic quiet phase, and the results show that the average rotation
247 rate of plasmasphere is about 90% of the corotational rate, in agreement with the
248 results of Lejosne and Mozer (2016). When the plasma elements rotate to the region
249 of 23:00 - 02:00 MLT, rotation rate in the outer plasmasphere reaches $\sim 130\%$ of
250 corotation, and in the inner plasmasphere is also close to the corotation rate. The
251 results show that the rotation rate of plasmasphere is overall increasing in the region.
252 In addition, the plasma elements in the outer plasmasphere rotate faster than the inner
253 plasmasphere in this region. The Fig.5(b) shows that rotation rate in the outer
254 plasmasphere highly reaches $\sim 140\%$ of corotation, and rotation rate in the inner
255 plasmasphere is close to 110% of corotation. So, we propose that the physical
256 mechanism of the shoulder formation is plasma extrusion of outer plasmasphere in the
257 predawn sector, due to outer plasmasphere both drifts radial outward and rotates faster.
258 In the present paper, the results show that the rotation rates of simulation are higher
259 than the observations, and not consistent with Huang et al. (2011) and Galvan et al.
260 (2010). The first reason is that this is a substorm case, so the convection of
261 magnetosphere is greater than the previous study articles of the geomagnetic quiet
262 case. (Galvan et al., 2010; Huang et al., 2011; Verbanac et al., 2018). The second

263 reason is that the Weimer electric field model is larger in practice, which results in a
264 larger total electric field value in calculation (Goldstein et al., 2002; Pierrard et al.,
265 2008).

266 The dawn-dusk asymmetry of convective electric field is caused by the terminal
267 conductivity gradient of the ionosphere. The subrotation of the ionosphere drives the
268 subrotation of the plasmasphere, and the plasmaspheric drift is correlated with the
269 phase of geomagnetic storm (Burch et al., 2004). The convection electric field of
270 Weimer (2001) is obvious dawn-dusk asymmetry, that causes a smaller increase on
271 the dawnside and a larger decrease on the duskside, indicating that the subrotational
272 effect of the plasmasphere is modulated by field-aligned current changes and
273 conductance variations (Liemohn et al., 2004). The asymmetry of potential pattern
274 causes the sunward convection in the magnetospheric night-side to be larger than that
275 in the morning side, resulting in the subcorotational flow in the dark side. (Gallagher
276 et al., 2005).

277

278 **5. Conclusion**

279 In this paper, we simulated the case of substorm on 8 June 2001 to investigate the
280 physical mechanism of the shoulder formation based on TPM model that utilizes
281 Weimer's electric field and the drift motion theory. We use the E-model and the
282 B-model that are quasi-static background field and global averages. So, the results of
283 simulation have some deviations with EUV observation. But, we have satisfactorily
284 reproduced the evolution and development of the features of the plasmopause, like the
285 shoulders and plumes. And then, the physical mechanism of the shoulder formation
286 has been investigated.

287 The formation of shoulder is associated with IMF northward turning in the predawn
288 sector. And the physical mechanism of shoulder formation is the result of plasma
289 extrusion in the predawn sector, caused by the fact that outer plasmasphere drifts
290 radially outward and rotates faster. The corotation rate in midnight sector decreases
291 with the increasing L-shell, while it increases in pre-dawn sector. So, the shoulder

292 forms across in the 03-06 MLT region.

293 The formation and evolution of plume and channel have also been reproduced in
294 this case. One can see single or double plumes appear in the dusk or afternoon sector,
295 then become thinner with time, and finally disappear.

296 In this model, we do not consider the refilling process of the ionosphere. In the
297 future work, the refilling process should be considered, and we expect to obtain more
298 reasonable results. And also, the physical mechanisms of plasmaspheric features
299 observed by EUV/IMAGE, like notch or channel, also are to be investigated by TPM
300 model in future work underway.

301 **Author contributions:** Zhang H. conceptualized the project and wrote the original
302 draft of the paper. Peng G. S. modified the Figures and coded the Fortran program. Shen
303 C. supervised the project, and reviewed and edited the paper. Wu Yewen gives some
304 suggestions and draws Figure 4 for the paper.

305

306 **Acknowledgment:** The author thanks the professor D. R. Weimer, who provided the
307 code of Weimer's electric field model and ACE satellite data center and Word Data
308 center for Geomagnetism, Kyoto provided observation data. The dataset of
309 EUV/IMAGE could be downloaded from the website <http://euv.lpl.arizona.edu/euv>.

310

311 **References**

312 Burch, J. L., Mende, S. B., Mitchell, D. G., Moore, T. E. , Pollock, C. J., Reinisch, B.
313 W., Sandel, B. R., Fuselier, S. A. , and Gallagher D. L.: Views of Earth's
314 magnetosphere with the IMAGE satellite, Science, 291, 691-624, doi:
315 10.1126/science.291.5504.619, 2001.

316 Carpenter, D. L. and Anderson, R. R.: An ISEE/Whistler model of equatorial
317 electron density in the magnetosphere, J. Geophys. Res., 97, 1097-1108,
318 doi:10.1029/91JA015481992, 1992.

319 Chen, A. J. and Wolf, R.A. : Effects on the plasmasphere of a time-varying convection
320 electric field, Planet. Space Sci., 20, 483-509, doi: 10.1016/0032-0633(72)90080-3,
321 1972.

322 Gallagher, D. L., Adrian, M. L. and Liemohn, M. W.: Origin and evolution of deep
323 plasmaspheric notches, J. Geophys. Res., 110, A09201, doi:10.1029/2004JA010906,
324 2005.

325 Galvan, D. A., Moldwin, M. B., Sandel, B. R., and Crowley, G. : On the cause of
326 plasmaspheric rotation variability: IMAGE EUV observation, J. Geophys. Res., 115,
327 A01214, doi:10.1029/2009JA014321, 2010.

328 Goldstein, J., Spiro, R. W., Reiff, P. H., Wolf, R. A., Sandel, B. R., Freeman, J. W., and
329 Lambour, R. L.: IMF-driven overshielding electric field and the origin of the
330 plasmaspheric shoulder of May 24, 2000, Geophys. Res. Lett., 29(16), 1819,
331 doi:10.1029/2001GL014534, 2002.

332 Grebowsky, J. M.: Model study of plasmopause motion, J. Geophys. Res., 75,
333 4329-4333, doi:10.1029/JA075i022p04329, 1970.

334 Huang Y., Xu, R. L., Shen, C., and Zhao H.: Rotation of the Earth's plasmasphere at
335 different radial distances, Adv. Space. Res., 48, 1167-1171, doi:
336 10.1016/j.asr.2011.05.028, 2011.

337 Lejosne, S., and Mozer, F. S. : Van Allen Probe measurements of the electric drift
338 $E \times B / B^2$ at Arecibo's L=1.4 field line coordinate, Geophys. Res. Lett., 43, 6768-6774,
339 doi: 10.1002/2016GL069875, 2016.

340 Li, L., and Xu, R. L.: Model of the evolution of the plasmasphere during a
341 geomagnetic storm, Adv. Space. Res., 36, 1895-1899. doi: 10.1016/j.asr.2003.10.057,
342 2005.

343 Nishida A.: Formation of plasmopause, or magnetospheric plasma knee, by the
344 combined action of magnetospheric convection and plasma escape from the tail, J.
345 Geophys. Res., 71, 5669-5679, doi:10.1029/JZ071i023p05669, 1966.

346 Pierrard V., and Lemaire, J. F.: Development of shoulders and plumes in the frame of
347 the interchange instability mechanism for plasmopause formation, Geophys. Res. Lett.,
348 31, L05809, doi:10.1029/2003GL018919, 2004.

349 Pierrard, V., and Cabrera, J.: Comparisons between EUV/IMAGE observations and
350 numerical simulations of the plasmopause formation, Annales Geophysicae, 23,
351 2635-2646, doi:10.5194/angeo-23-2635-2005, 2005.

352 Pierrard, V., and Cabrera, J.: Dynamical simulations of plasmopause deformations,
353 Space.Sci.Res, 122, 119-126, doi: 10.1007/s11214-006-5670-3, 2006.

354 Pierrard, V., Khazanov, G. V., Cebreira, J., and Lemaire, J.: Influence of the convection
355 electric field models on predicted plasmopause positions during magnetic storms. J.
356 Geophys. Res. 113, A08212, doi:10.1029/2007JA012612, 2008.

357 Sandel, B. R., King, R. A., Forrester, W. T., Gallagher, D. L., Broadfoot, A. L., and
358 Curtis, C. C.: Initial results from the IMAGE extreme ultraviolet imager, Geophys.
359 Res. Lett., 28, 1439, doi: 10.1029/2001GL012885, 2001.

360 Verbanac, G., Bandic, M., Pierrard, V., and Cho, J.: MLT plasmopause characteristics:
361 Comparison between THEMIS observations and numerical simulations. J. Geophys.
362 Res: Space physics, 123, 2000-2007, doi:10.1002/2017JA024573, 2018.

363 Weimer, D. R.: An improved model of ionospheric electric potentials including
364 substorm perturbations and application to the Geospace Environment Modeling
365 November 24, 1996, event., J. Geophys. Res., 106, 407-416,
366 doi:10.1029/2000JA000604, 2001.

367 Zhang, H., Xu, R. L., Zhao, H., and Shen, C.: The characteristics of the model of
368 Weimer's electric field within the magnetosphere., Chinese J. Geophys. 55, 36-45, doi:
369 10.6038/j.isnn.0001-5733.2012.01.004, 2012.

370 Zhang, H., Xu, R. L., Shen, C., and Zhao, H.: The simulation of the plasmaspheric
371 morphology during a magnetospheric disturbance event, Chin J. Geophys, 56,
372 731-737, doi:10.6038/cjg 20130302, 2013.